PCCP

PAPER

Cite this: *Phys. Chem. Chem. Phys.*, 2016, **18**, 6217

P3HT:DiPBI bulk heterojunction solar cells: morphology and electronic structure probed by multiscale simulation and UV/vis spectroscopy†

Thorsten Winands,*[a] Marcus Böckmann,[a] Thomas Schemme,[b] Phong-Minh Timmy Ly,[a] Djurre H. de Jong,[c] Zhaohui Wang,[d] Cornelia Denz,[b] Andreas Heuer[c] and Nikos L. Doltsinis[a]

Received 3rd November 2015,
Accepted 2nd February 2016

DOI: 10.1039/c5cp06704a

www.rsc.org/pccp

Coarse grained molecular dynamics simulations are performed for a mixture of poly(3-hexylthiophene) (P3HT) and diperylene bisimide (DiPBI). The effect of different annealing and cooling protocols on the morphology is investigated and the resulting domain structures are analyzed. In particular, π-stacked clusters of DiPBI molecules are observed whose size decreases with increasing temperature. Domain structure and diffusivity data suggest that the DiPBI subsystem undergoes an order → disorder phase transition between 700 and 900 K. Electronic structure calculations based on density functional theory are carried out after backmapping the coarse grained model onto an atomistic force field representation built upon first principles. UV/vis absorption spectra of the P3HT:DiPBI mixture are computed using time-dependent density functional linear response theory and recorded experimentally for a spin-coated thin film. It is demonstrated that the absorption spectrum depends sensitively on the details of the amorphous structure, thus providing valuable insight into the morphology. In particular, the results show that the tempering procedure has a significant influence on the material's electronic properties. This knowledge may help to develop effective processing routines to enhance the performance of bulk heterojunction solar cells.

I. Introduction

Organic photovoltaic devices typically employ a mixture of a polymer species, *e.g.* poly(3-hexylthiophene) (P3HT), acting as an electron donor (D) and a fullerene derivative, *e.g.* [6,6]-phenyl-C_{61} (or C_{71})-butyric acid methyl ester (PCBM), acting as an acceptor (A).[1–4] Although fullerene-based bulk heterojunction solar cells have achieved considerable progress in recent years, reaching power conversion efficiencies (PCEs) of over 8.5% (see, for instance, ref. 5), there is still a need for further improvement, in particular with regards to light absorption and production cost. A number of alternatives to fullerene-based acceptors have been proposed recently,[6–23] with much of the research focussing on perylene bisimide (PBI) derivatives. Due to these efforts, the PCEs of non-fullerene devices have steadily increased to about 5% over the past few years. To further improve their efficiency, the non-fullerene acceptors need to be matched with suitable donor polymers resulting in favourable morphologies of the donor/acceptor mixture. While the importance of the morphology for the overall device performance is undoubted, the details of the relationship between the atomistic D–A bulk structure and its electronic properties have not yet been fully established. This is partly due to the difficulty in characterizing the microstructure experimentally. Atomic force microscopy has been employed successfully to unravel the size and shape of donor and acceptor domains. However, this technique does not provide any information on molecular conformation or the type of molecular aggregates formed.

This is where theoretical analyses and reliable predictions are most valuable to guide future device fabrication. From a computational point of view, the problem is complicated as it involves several interlinked layers of theory at different scales. Clearly, electronic structure calculations are quantum-mechanical and, due to the computational effort required, only applicable to small systems (on the nanometer scale, at best).

[a] *Institut für Festkörpertheorie, Westfälische Wilhelms-Universität Münster and Center for Multiscale Theory & Computation, Wilhelm-Klemm-Str. 10, 48149 Münster, Germany. E-mail: t.winands@wwu.de*
[b] *Institut für Angewandte Physik, Westfälische Wilhelms-Universität Münster, Corrensstr. 2/4, 48149 Münster, Germany*
[c] *Institut für Physikalische Chemie, Westfälische Wilhelms-Universität Münster and Center for Multiscale Theory & Computation, Corrensstr. 28/30, 48149 Münster, Germany*
[d] *Beijing National Laboratory for Molecular Sciences, Institute of Chemistry, Chinese Academy of Sciences Beijing, 100190, P. R. China*

† Electronic supplementary information (ESI) available. See DOI: 10.1039/c5cp06704a

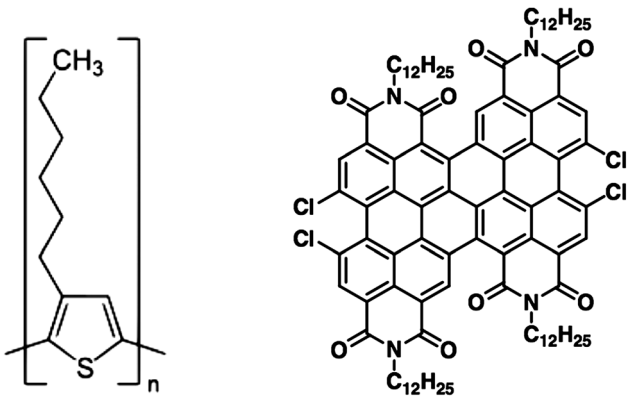

Fig. 1 Left: Chemical structure of poly(3-hexylthiophene) (P3HT), where *n* is the number of repeat units. Right: Chemical structure of perylene bisimide dimer (DiPBI).

Morphology simulations, on the other hand, demand micrometer length scales and microsecond time scales. Hence an overall theoretical description calls for a multiscale approach.[24,25] In the field of organic photovoltaics, such kind of multiscale simulations have been pioneered by Andrienko, Nelson and others.[26–31]

In this paper, we present multiscale computations on a prototypical P3HT:DiPBI non-fullerene bulk heterojunction (see Fig. 1 for the respective chemical structures). The first step consists in coarse grained molecular dynamics (CG-MD) simulations of the bulk mixture to study its general morphology and the formation of donor and acceptor domains, in particular. Here, the effect of different annealing protocols on the morphology is investigated as it is known that annealing can significantly improve the device performance. After the CG-MD simulations, the respective structures are backmapped onto an atomistic molecular mechanics (MM) representation and re-equilibrated in an MM-MD run. From the final MM-MD structure, individual molecules (and pairs) are extracted to perform electronic structure calculations using density functional theory (DFT). In particular, we use time-dependent DFT linear response theory (TDDFT) to calculate UV/vis spectra of the materials. For comparison, we record experimental UV/vis spectra of spin-coated thin films of the P3HT:DiPBI mixture, but also of pure P3HT and DiPBI, subjected to different annealing protocols. The aim is firstly to establish a relation between the UV/vis spectra and the underlying morphology and molecular conformation, as has been successfully demonstrated in the case of pure P3HT.[25,32] Secondly, the insights gained from the present studies could be useful to develop optimized tempering protocols to enhance the electronic properties of organic solar cells.

II. Computational details

A. Coarse grained molecular dynamics simulations

All coarse grained molecular dynamics runs were performed with the Gromacs 5.0.x software package.[33,34] The production runs were carried out in the *NPT* ensemble using a leap-frog integrator with a timestep of 20 fs. To control the temperature, the velocity rescaling temperature coupling with a stochastic term[35] was used, which would ensure a proper canonical ensemble in an *NVT* simulation. Isotropic pressure coupling was realized using the Parrinello–Raman algorithm[36] with a time constant of 12.0 ps for a target pressure of 1 bar and a compressibility of 3.0×10^{-4}. Neighbor lists were built using the Verlet cutoff scheme with a cut-off radius of 1.1 nm, and updated at each step.

The coarse graining (or 'mapping') of the atomistic structure was done with a modified version of the initram.sh script, which calls the backward.py script, by Wassenaar *et al.*[37,38] The CG topologies are based on the Martini force field.[38,39] Parameters for P3HT are employed as described in.[32] In short, the molecule is described by three particles and one virtual site for the thiophene ring, and two particles for the hexyl chain (see Fig. 2 (left); reference values and force constants for bond length and bond angle potentials are listed in the ESI†). The virtual site is massless, has no LJ interaction with other beads, and is positioned at the center of mass of the three ring particles. Introducing a virtual site is a means to increase numerical stability. The triangle of constraints in the backbone ring would otherwise be difficult to solve and very sensitive to forces from connected beads. This is alleviated by spreading the forces *via* the virtual site over the underlying atoms.

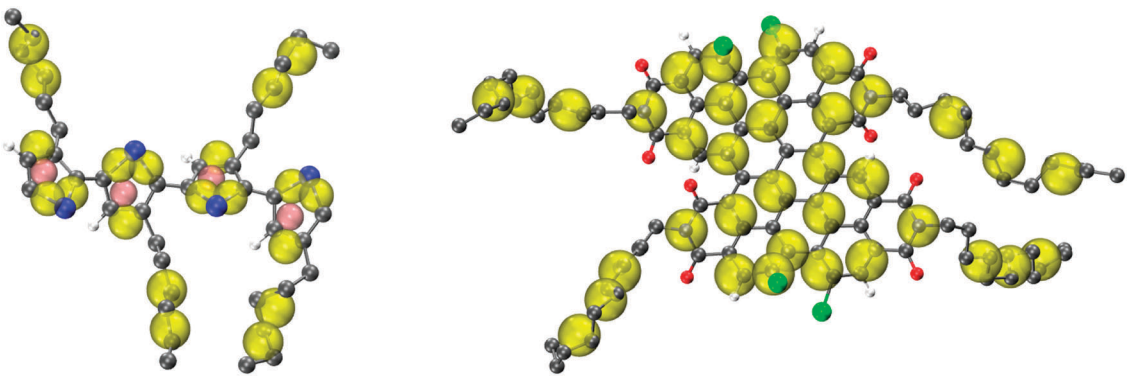

Fig. 2 Left: Snapshot of the CG representations of P3HT (four thiophene units are shown). Each monomer consists of five CG beads (yellow) and one virtual site (pink). Right: Snapshot of the CG representation of DiPBI.

In order to correctly reproduce the density and stacking of the crystal,[40] the LJ σ value for the self-interaction is reduced from 0.47 to 0.43 nm for the tail particles and to 0.32 nm for the ring particles (S- and T-type particles in the Martini force field, respectively).[32]

In the P3HT molecule there are three different kinds of angles as shown in Table S2 in the ESI.† The dihedrals in P3HT were set to a reference value of 0° with a force constant of 1.8 kJ mol^{-1} for multiplicity 1 and a force constant of −9.5 kJ mol^{-1} for multiplicity 2.

The DiPBI molecule is also described by three types of particles (Fig. 2, right). The nitrogen atoms bearing the hydrocarbon side chains are represented by a SP3 bead each (please note that the notation SP3 purely refers to the Martini bead type and not to the hybridization state of the nitrogens). The four hydrocarbon side chains are each described by three SC1 beads, and the carbon ring structures including the chlorine atoms are formed by a total of 20 TC4 beads. The reference values and force constants between the different types of beads are listed in Table S3 in the ESI.† The non-bonded interactions of were parametrized in such a way as to conserve the particle density from the MM representation. In particular, the π-stacked DiPBI dimer motif was parametrized against an MM optimized structure, which in turn was parametrized against DFT calculations.

The initial CG structure was obtained by mapping a pre-equilibrated atomistic structure containing 1248 DiPBI and 416 P3HT molecules with a chain length of 32 thiophene units. The 3 : 1 number ratio of DiPBI to P3HT molecules was chosen to approximately reproduce the mass ratio of 1 : 1 used in the experimental samples. Please note that the mean repetition length of the P3HT oligomers used in our experiments is 252. However, both the MD simulations and the electronic structure calculations (see below) would be infeasible with P3HT molecules of this length. The pre-equilibration of the MM system consisted of a 1 ns run at 600 K, followed by a 5 ns run at 300 K using a Berendsen thermostat and a timestep of 1 fs. In view of the much longer CG equilibration to follow, the MM pre-equilibration phase is of minor importance; it served mainly to increase the initial numerical stability of the CG run.

In the CG representation, the system was then further equilibrated for 200 ns at 700 K, then cooled down to 500 K at a rate of 4 degrees per ns. Once the temperature of 500 K was reached, three productions runs—at 500 K, 700 K, and 900 K—were initiated, each spanning a duration of 1 μs. For the runs at 700 K and 900 K, this included a short equilibration period at the respective temperature.

At the end of each run, *i.e.* after 1 μs, the system was cooled down to 300 K instantly by adjusting the target temperature and run for an additional 100 ns before subsequent backmapping, analysis, and quantum-mechanical calculations.

B. Atomistic molecular dynamics simulations

All atomistic molecular dynamics runs were performed with the Gromacs 5.0.x program[33,34] using a Gromos 45a3-based force field specifically tailored to match DFT results. In the case of P3HT, this includes atomic point charges distinguishing head, tail, and central thiophene units and a torsional potential between adjacent thiophene rings adapted as to reproduce B3LYP/6-31G* reference data for the minimum energy path along the SCCS dihedral for the dimer. More details regarding the parametrization can be found in.[32]

The topology for DiPBI was initially built using the Automated Topology Builder[41–43] based on a Gromos 54a7 force field. The DiPBI topology can be found in the ESI.† The force field representation has been validated against results from static and dynamic DFT calculations.

The atomistic MD runs were initiated by carefully backmapping from the CG simulations (see above) following a multi-step procedure with increasing level of pair interactions as made available by the 'initram.sh' script of Wassenaar *et al.*[37,38] First, atoms were projected around the bead positions. Second, two consecutive geometry optimizations with 500 steps each were performed, with nonbonded cutoffs of 0.1 nm and 1.0 nm, respectively. Subsequently, a series of six *NVT* simulations with increasing timestep (from 0.1 fs to 0.5 fs) and temperature (from 1 K to 300 K) were carried out. In order to ensure a good match to the CG structure, position restraints were used, typically in the backbone of the molecules. For the first three simulations, the velocity rescale thermostat[35] was chosen, while the Berendsen thermostat was used for the last three. All six simulations were run for 10 000 steps.

After this multistep backmapping procedure, the systems were simulated for another 150 ps at 300 K in the *NVT* ensemble using a timestep of 0.5 fs and a Berendsen thermostat.

C. Density functional theory calculations

All density functional theory (DFT) calculations were performed with the Gaussian 09 Rev. D.01 quantum chemistry package.[44] By default the absorption spectra were calculated using the time-dependent DFT (TDDFT) linear response method with the PBE0[45] exchange–correlation functional and the 6-31G* basis set. In each TDDFT calculation, the lowest 80 excited singlet states were computed. For the overall spectrum of the P3HT:DiPBI mixture, we averaged over 10 single molecule spectra of each species of randomly selected molecules from the final structure of the backmapped atomistic MD runs. The averaged DiPBI spectrum was weighted by a factor of three to reflect the mole ratio of 3 : 1 of the DiPBI : P3HT mixture. Lorentz broadening with a full width at half maximum of 20 nm was applied to the line spectra of the individual molecules.

III. Experimental details

All experimental investigations are based on a commercially available P3HT (Plexcore OS 2100) with an average molecular weight of M_n = 64.5 ± 10.5 kDa and on tetrachlorinated diperylene bisimide (C12-4ClDiPBI).[10]

For the determination of thin film absorbance of layers of P3HT and DiPBI solutions in chloroform at a concentration of 10 mg ml^{-1} were prepared, respectively. Both solutions were stirred for 3 hours, then heated to (45 ± 5) °C for ten minutes,

and afterwards filtered through a 0.45 PTFE syringe filter. Based on these solutions, a 1 : 1 mixture of P3HT and DiPBI was produced. Thin films of P3HT, DiPBI, and P3HT : DiPBI were fabricated by means of spin coating of the solutions onto microscope slides. The spinning speed was adjusted to 10 rps.

The influence of intense annealing on the film morphology was carried out by heating the samples to (450 ± 30) °C or (250 ± 30) °C on a hot plate for 20 s and followed by rapid cooling down to room temperature by putting them onto a solid block of copper.

Absorption spectra of the films were taken prior and post annealing by a Jasco V-530 UV/Vis spectrometer with an additional mask in the beam path to seize the illuminated area of each sample.

IV. Results and discussion

A. Morphology

Let us begin with a visual inspection of the blend morphologies resulting from the three different simulation protocols. In order to provide a better view inside the bulk structure, Fig. 3 shows equidistant, 2 nm thick, slices cut out of the respective unit cells at the end of the CG simulations at 500, 700, and 900 K, whereas a front view of the slices is depicted in Fig. 4. The immediate observation is that two different species, displayed in contrasting colors (outer layers: P3HT (yellow), DiPBI (pink), middle layer: P3HT (green), DiPBI (purple)), form sizable domains, *i.e.* they do not mix perfectly. The expansion of the unit cell with increasing temperature after the 1 μs annealing period is clearly visible. Fig. 4 reveals that the amount of 'empty space' indeed grows significantly with rising temperature. While there are no visible gaps in the amorphous structure at 500 K, small white areas start to appear at 700 K, which are noticeably expanded at 900 K. At all temperatures the DiPBI molecules are seen to form ordered π stacks, whereas the P3HT oligomers form large interconnected disordered domains. Visual inspection already points to a marked difference in the domain sizes at 900 K compared to 500 and 700 K. As can be seen from Fig. 4, the domains are broken up into much smaller parts at 900 K. This is indicative of a order → disorder phase transition between 700 and 900 K. The temperature-dependent diffusion behavior of the blend will be discussed in detail below (see Section IV.B). It is, however, known from the literature that pure P3HT melts around 500 K, depending on the molecular weight of the polymer.[46] Our own DSC measurements yield a melting temperature of 485 K for pure samples of amorphous P3HT. A P3HT:PCBM mixture was found to melt at 560 K.[46] Melting temperatures between 506 and 655 K have been measured experimentally for perylene diimide derivatives.[47] The value of 537 K determined by us for pure DiPBI also lies in that range. Disordering temperatures between 633 and 693 K have been reported for perylene diimide derivatives,[47] while our CG simulations suggest a value above 700 K in the case of DiPBI.

Upon cooling the systems to 300 K, the volume of the unit cell shrinks expectedly and the voids in the morphology previously seen at 700 K and particularly at 900 K disappear (see Fig. 5). Nevertheless, as can be seen, important differences in the domain structure remain. This is largely due to the rapid quenching of the systems, which essentially preserves the main characteristics of the annealed morphology.

In the following we will perform a quantitative analysis of the domain structures. Since P3HT does not form enclosed domains but rather a large network of interconnected assemblies, we will focus here on the DiPBI domains. To define a domain, we have used two different criteria:

- Criterion I counts DiPBI molecules as belonging to the same domain, if their center-of-mass (COM) distance is below 20.0 Å, which is large enough to register two DiPBI molecules sitting side by side, and in addition any two CG beads are within 6.0 Å of each other.
- Criterion II counts DiPBI molecules as belonging to the same domain, if their COM distance is below 20.0 Å and in addition any two CG beads are within 4.0 Å of each other. This way, only individual π-stacks are counted.

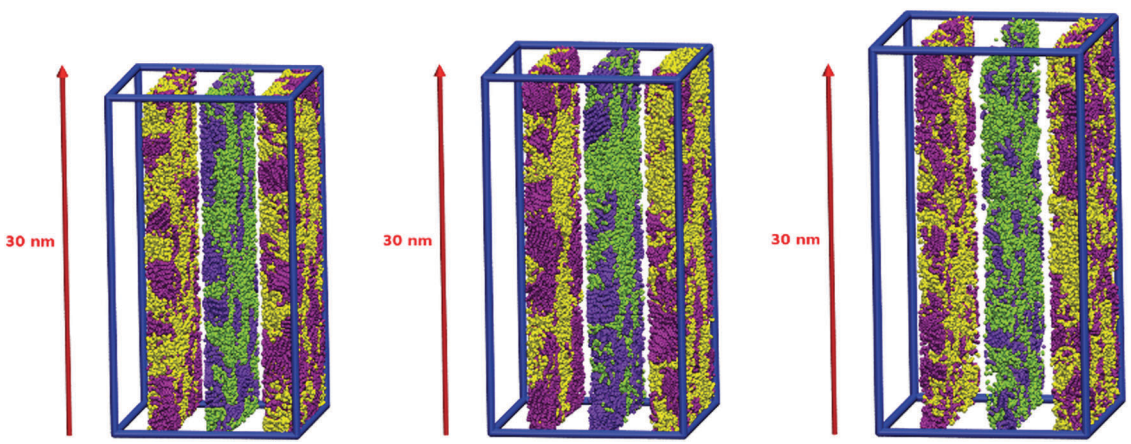

Fig. 3 Final structure of the simulations at 500 K (left), 700 K (middle), and 900 K (right) cut into three equidistant slices of 2 nm thickness to provide a better view inside the bulk. In the two outer slices, DiPBI molecules are shown in pink, P3HT molecules in yellow. In the middle slice, DiPBI molecules are presented in purple, P3HT molecules in green.

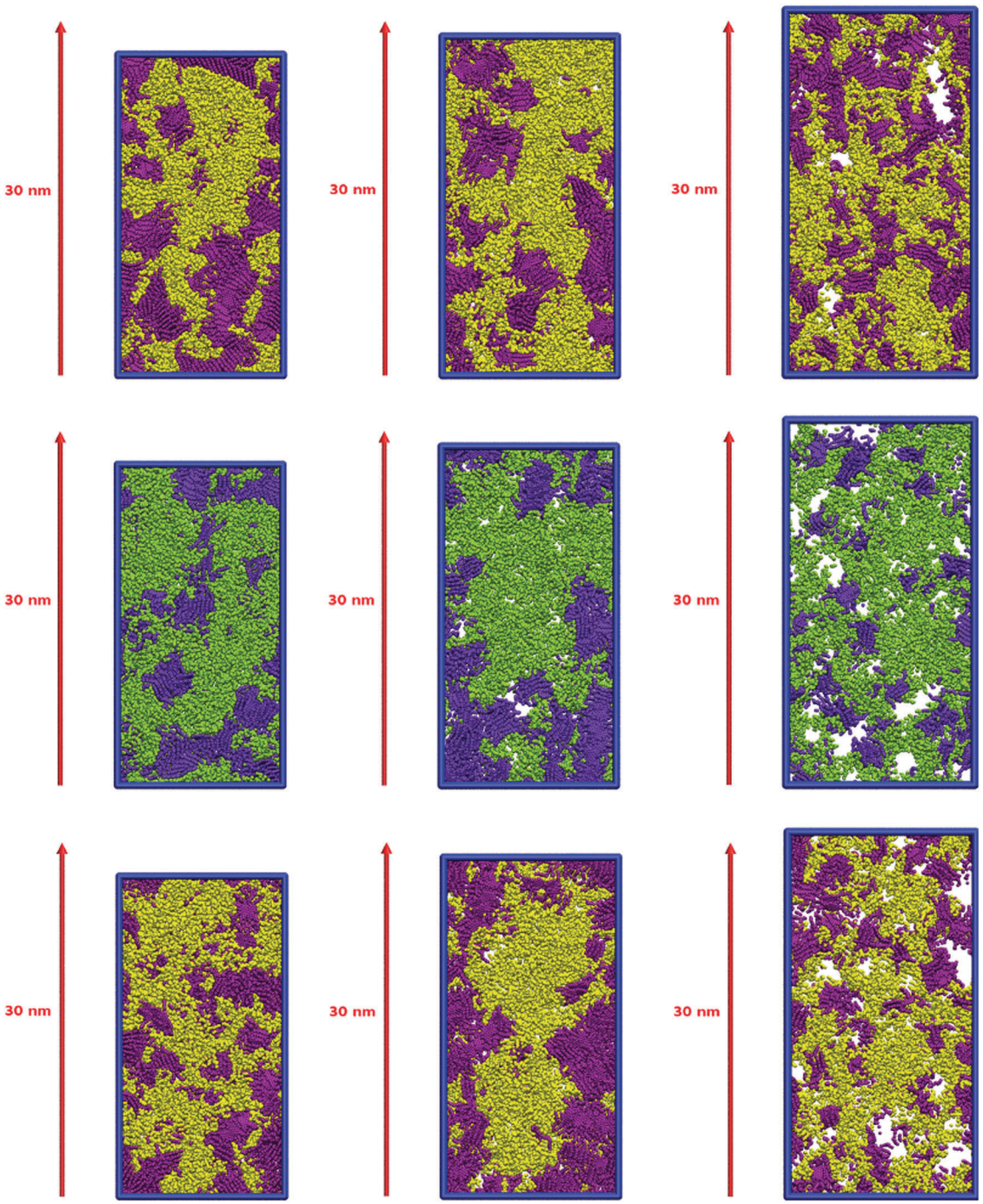

Fig. 4 Front view of all slices shown in Fig. 3. Left column: 500 K, middle column: 700 K, right column: 900 K. In the top and bottom rows, DiPBI molecules are shown in pink, P3HT molecules in yellow. In the middle row, DiPBI molecules are represented in purple, P3HT molecules in green.

Fig. 6 shows a histogram of the DiPBI domain sizes according to criterion I. The distributions are seen to be fairly broad with domain sizes ranging from 1 to 15 molecules. It is apparent that the domains are typically smaller at 900 K compared to 700 K and 500 K, which is plausible because of the high mobility in the melted structure. What is a little surprising is the fact that the simulation at 700 K seems to produce more larger domains than the 500 K simulation. The reason for this could be partly that at 500 K the system is practically frozen on the simulation time scale and therefore molecules are not sufficiently mobile to aggregate into larger domains. On the other hand, we have performed an additional analysis of the time-evolution of the domain size distribution (see ESI,† Fig. S3), revealing that small fluctuations do occur at both temperatures and on average the distributions at 500 and 700 K are very similar.

Interestingly, the distributions change only moderately upon cooling the systems to 300 K, which is probably due to

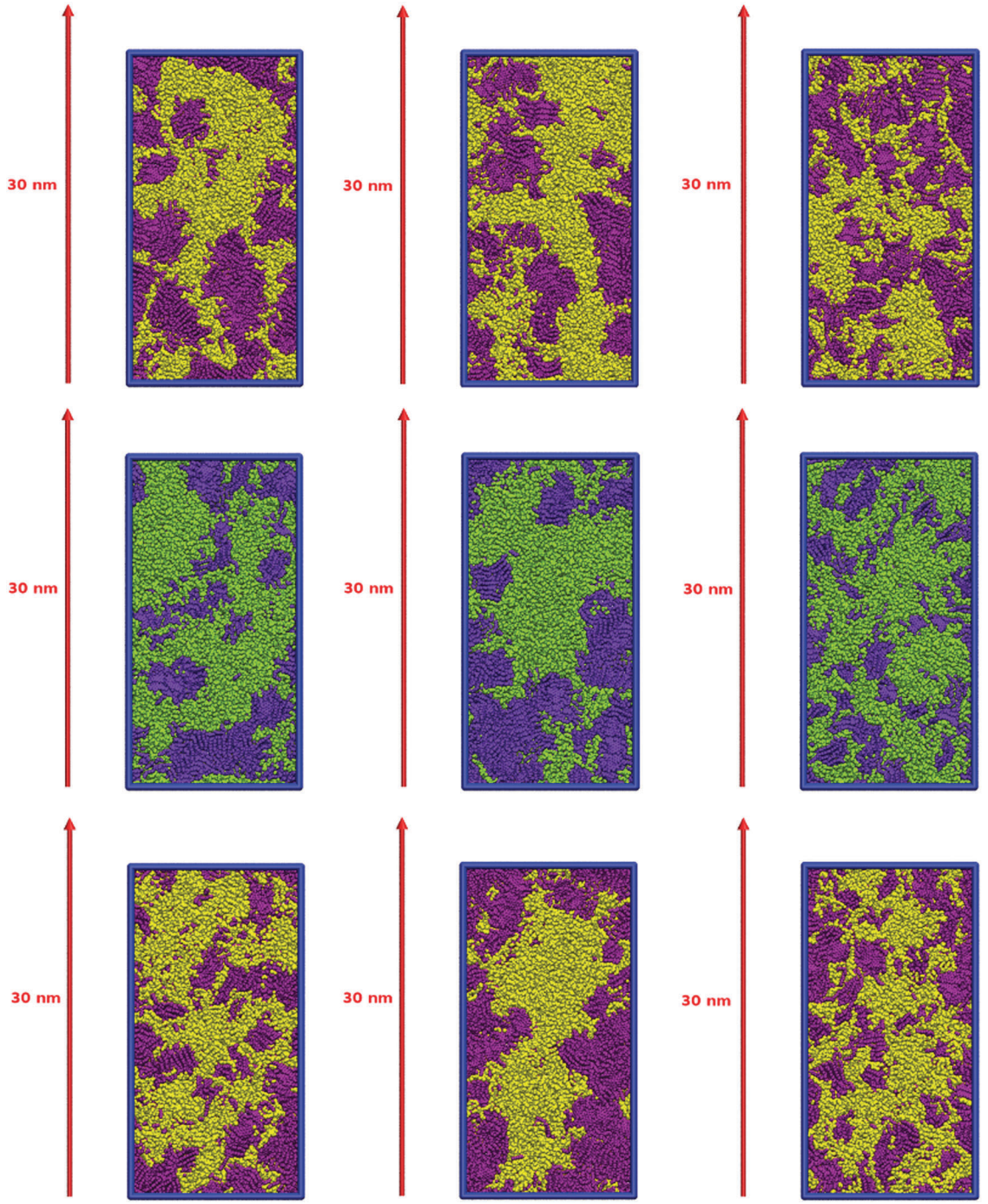

Fig. 5 Front view of all slices shown in Fig. 3 after cooling the systems to 300 K. Left column: 500 K, middle column: 700 K, right column: 900 K. In the top and bottom rows, DiPBI molecules are shown in pink, P3HT molecules in yellow. In the middle row, DiPBI molecules are represented in purple, P3HT molecules in green.

the rapid quenching, essentially 'freezing' the hot state. Further analysis shows that the quenched domain size distribution is still in the range of the time-dependent fluctuations occurring in the 500 K simulation (see ESI,† Fig. S3). We have also carried out an additional simulation in which the system was slowly cooled at a rate of 1 degree per ns, again yielding a similar distribution. It should be stressed at this point that even this slow cooling rate is orders of magnitude faster than the relevant lab time scales, which are on the order of seconds or minutes. However, this is a problem of MD methods in general.

The domain size distribution obtained with criterion II is shown in Fig. 7. It is immediately apparent that this domain definition leads to much smaller domains compared to criterion I (Fig. 7). Before cooling the largest domain contains 9 DiPBI molecules at 500 K, 10 at 700 K, and 7 at 900 K. This is because criterion II predominantly assigns DiPBI molecules in

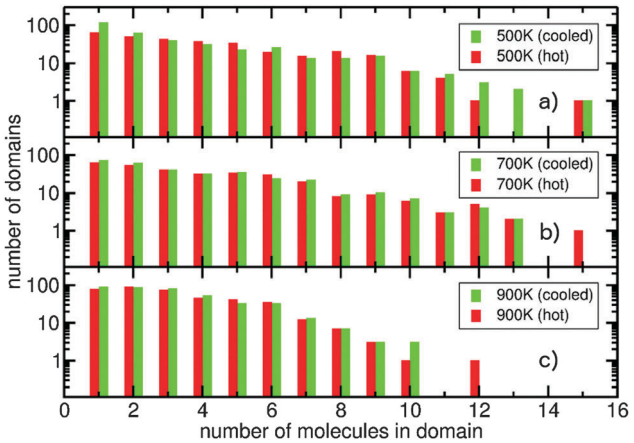

Fig. 6 Domain size histograms according to criterion I for the final structures of the 500 K (a), 700 K (b), and 900 K (c) runs before (red) and after (green) cooling to 300 K.

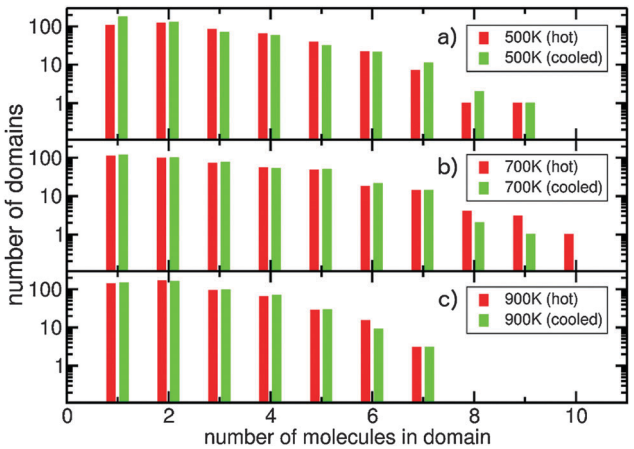

Fig. 7 Domain size histograms according to criterion II for the final structures of the 500 K (a), 700 K (b), and 900 K (c) runs before (red) and after (green) cooling to 300 K.

a single π-stack to a certain domain, whereas criterion I also allows two or more adjacent stacks to be part of a single domain (as illustrated by Fig. 8). The trends with respect to temperature, however, remain the same as for criterion I.

Although we have focussed above on π-stacked DiPBI molecules, we have also investigated the role of hydrogen bonding by calculating Cl···H and O···H radial distribution functions. From this analysis we conclude that the average number of hydrogen bonds is only a fraction of one per acceptor. In addition, the majority of them are highly nonlinear and arise from close contacts within π-stacked DiPBI arrays. Thus π-stacking is clearly the dominant factor in structure formation here.

B. Mobility

The extent to which domain boundaries and sizes can change over time depends on the mobility of the constituent molecules. A measure for the mobility is their mean square displacement (MSD) as a function of time. Fig. 9 shows the MSD curves for

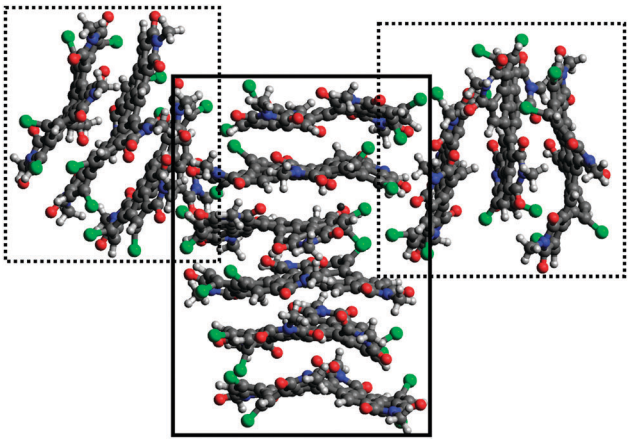

Fig. 8 Example of a domain determined according criterion I (solid and dashed boxes) and II (solid box).

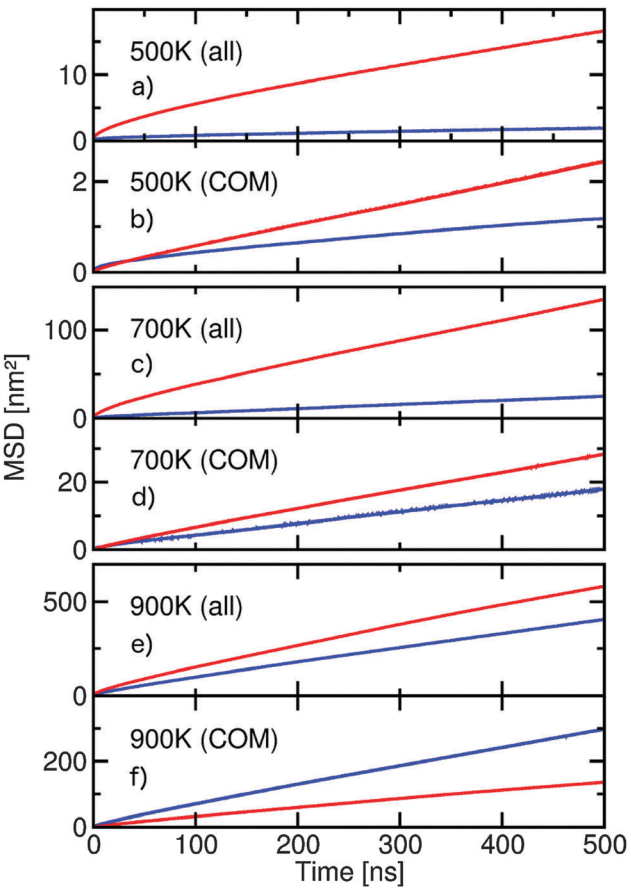

Fig. 9 Ensemble and time averaged mean square displacement as a function of time for DiPBI (blue lines) and P3HT (red lines) at 500 K (a, b), 700 K (c, d) and 900 K (e, f). Curves labeled with AA have been obtained using the positions of all beads, while those labeled with COM only consider center-of-mass motion.

P3HT and DiPBI for the annealed systems at 500, 700, and 900 K. In each case, two curves are presented—one considering only the COM and the other taking into account all CG beads of the particular species. By comparing the two, one can obtain information on conformational and rotational motion.

From the all-particle curves in Fig. 9a it appears that at 500 K, P3HT diffuses faster than DiPBI by an order of magnitude. Only the comparison to the all-particle to the COM curves (Fig. 9b) reveals that the P3HT all-particle curve contains predominantly intramolecular contributions caused by large conformational changes of the polymers. In fact, the COM curves of the two species are rather similar. However, the slope of the P3HT curve is still roughly twice as large as that for DiPBI. This could be due to the fact that the simulation temperature of 500 K lies above the melting point of P3HT (485 K), while it is just below that of DiPBI (537 K). As we know from the domain structure analysis above, the DiPBI molecules are mainly present in π-stacks, which would explain their reduced mobility.

The picture is qualitatively unchanged at 700 K (Fig. 9c and d). As for 500 K, the all-particle diffusion of P3HT is much faster than that of DiPBI, whereas the COM curves start out almost on top of each other with DiPBI being slightly slower overall. For both types of molecules the slope and thus the diffusivity has increased by an order of magnitude compared to 500 K.

At 900 K, the situation finally changes drastically (Fig. 9e and f). The large difference between the all-particle curves of P3HT and DiPBI prevalent at the lower temperatures has all but disappeared (Fig. 9e). For the first time, the COM diffusion of DiPBI is faster than that of P3HT. This is in line with the above analysis of the domain structure, which implied that a temperature of 900 K leads to the break-up of larger DiPBI domains into smaller, more mobile, stacks and single molecules. The MSD data clearly support the idea of an order → disorder phase transition in the DiPBI subsystem between 700 and 900 K.

C. Absorption spectra

It is known from pure P3HT that the UV/vis absorption spectrum sensitively depends on temperature and thermodynamic phase due to changes in the underlying molecular structure.[25,32] In the following, we analyze the optical absorption spectrum of the P3HT:DiPBI mixture, as it may hold valuable clues on the microscopic structure of the bulk heterojunction material. Let us start by looking at the experimental spectrum obtained for a spin-coated thin film. Fig. 10 shows the UV/vis spectrum of a P3HT:DiPBI thin film together with the spectra of pure P3HT and DiPBI thin films. The P3HT:DiPBI spectrum has three distinct peaks at about 410, 510, and 670 nm which can be clearly assigned to the P3HT and DiPBI components by comparison with the spectra of the respective pure films. The main broad feature at 510 nm corresponds to the characteristic P3HT thin film spectrum, while the other two peaks originate from DiPBI.

We therefore begin our theoretical analysis with the spectra of the individual components. Fig. 11 shows the theoretical averaged DiPBI spectra of the P3HT:DiPBI mixture from the 500, 700, and 900 K simulations quenched to 300 K. The theoretical 500 K spectrum is seen to have a very similar shape as the experimental spectrum, however it is red-shifted by about 50 nm. We would like to stress that this shift is likely to be a temperature effect rather than an error due to the DFT method chosen, since the spectrum obtained for the optimized geometry agrees well with experimental one (see ESI,† Fig. S5).

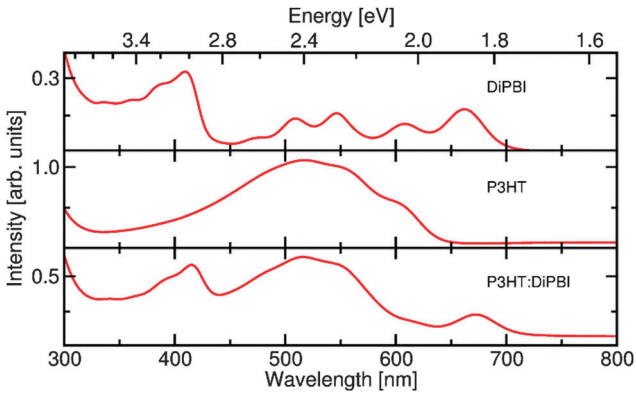

Fig. 10 Experimental absorption spectra of spin-coated thin films of pure DiPBI (top), pure P3HT (middle), and a P3HT:DiPBI mixture (bottom).

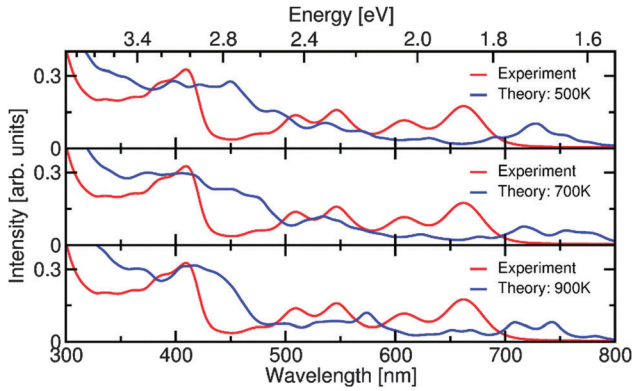

Fig. 11 Theoretical absorption spectra of DiPBI within the P3HT:DiPBI mixture quenched to 300 K from simulations at 500 (top), 700 (middle), and 900 K (bottom) together with the experimental spectrum of a pure DiPBI thin film at 300 K.

Test calculations have shown that the double peak structure at 500/550 nm and 600/650 nm of the experimental spectrum is in fact due to dynamical effects by averaging TDDFT spectra along a single molecule trajectory, whereas the optimized structure only yields two single peaks. The theoretical peak at 720 nm is seen to get weaker when the temperature is increased to 700 and 900 K, while the contributions between 750 and 800 nm become stronger. Overall, the differences between the three temperatures are, however, relatively minor, which is plausible given the rigidity of the DiPBI molecule. At the same time, this suggests that environmental effects, for instance caused by π-stacking or the interaction with P3HT, play a more subtle role.

To further investigate the effect of temperature on the absorption spectra, we have performed UV/vis spectroscopy on spin-coated thin films of pure DiPBI at 573 and 773 K (see Experimental details section). Fig. 12 compares the spectra obtained at the two elevated temperatures with the one at 300 K. The peaks expectedly become broader with increasing temperature and a slight red-shift can also be observed, which is line with the theoretical spectra from the annealed simulations (Fig. 11).

The absorption spectrum of the P3HT subsystem of the P3HT:DiPBI mixture contains additional information on the

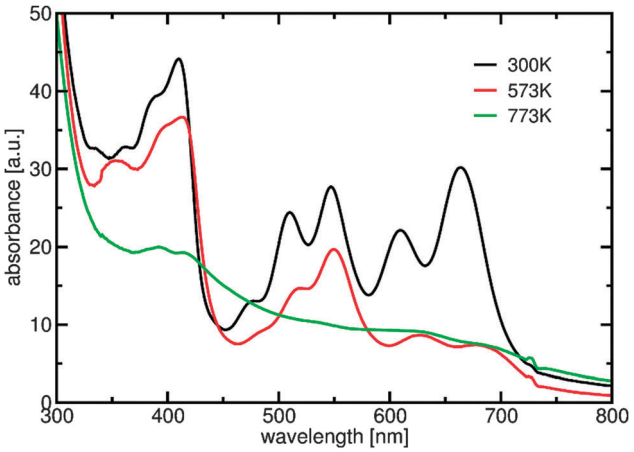

Fig. 12 Experimental absorption spectra of spin coated DiPBI thin films at 300 (black), 573 (red), and 773 K (green).

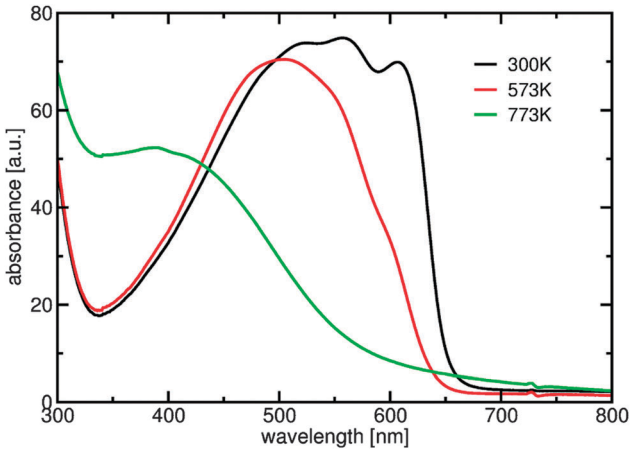

Fig. 14 Experimental absorption spectra of spin-coated P3HT thin films at 300 (black), 573 (red), and 773 K (green).

amorphous structure. Fig. 13 shows the calculated averaged P3HT spectra for the quenched 500, 700, and 900 K runs and compares them to the experimental spectra obtained in previous work on pure P3HT in a thin film and a chloroform solution.[32] The 500 K spectrum can be described as a superposition of the thin film and the solution spectrum of pure P3HT. As discussed above (see, for example, diffusion properties) the P3HT subsystem is—at least partially—liquid. During rapid quenching to 300 K, the system is essentially frozen in this partially liquid state. It is possible that certain regions become more like an amorphous solid in the process. This might be enhanced in the vicinity of the DiPBI domains, which are still frozen at 500 K.

It can be seen that the amorphous solid contribution around 500 nm diminishes with increasing temperature (Fig. 13 middle and bottom panel) and the solution-like peak at just over 400 nm becomes dominant. Comparing the three simulations clearly suggests that different annealing and cooling protocols can generate a range of different morphologies and aggregation states with varying electronic properties. To verify the theoretical prediction, we have also measured experimental absorption spectra of spin-coated thin films of P3HT subjected to different annealing temperatures (see Experimental Details Section). The experimental UV/vis spectra at 300, 573, and 773 K shown in Fig. 14 strongly support the theoretical data in so far as they indeed exhibit a pronounced blue-shift with increasing temperature.

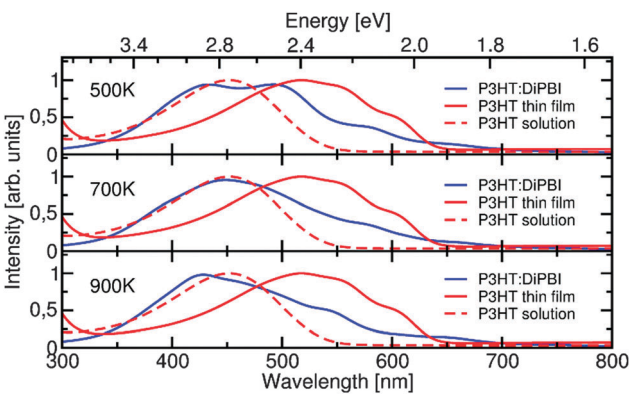

Fig. 13 Theoretical absorption spectra of P3HT within the P3HT:DiPBI mixture at 500 (top), 700 (middle), and 900 K (bottom) together with the experimental spectra of a pure P3HT thin film (solid red lines) and P3HT in chloroform solution (dashed red lines).

V. Conclusions

Multiscale simulations have been performed of a P3HT:DiPBI mixture exposed to different annealing and cooling protocols using a combination of coarse grained molecular dynamics, atomistic molecular dynamics, and density functional theory based electronic structure calculations. Analysis of the morphology has revealed a pronounced domain structure. In particular at 500 and 700 K large clusters of π-stacked DiPBI molecules were found. At 900 K—above the order → disorder phase transition of DiPBI—these stacks were seen to break up into smaller parts.

The notion that P3HT is molten in the 500 to 900 K temperature interval, while DiPBI melts above 500 K and shows an order → disorder phase transition somewhere between 700 and 900 K, is supported by a diffusivity analysis. The mean square displacement of DiPBI was seen to overtake that of P3HT between 700 and 900 K.

Optical absorption spectra have been calculated by averaging over individual molecules sampled from the three systems quenched to 300 K and compared to experimental UV/vis spectra recorded for thin films. The theoretical spectrum of the DiPBI subsystem has a similar shape as the experimental spectrum of pure DiPBI, but is slightly red-shifted. The calculated P3HT spectrum is found to become increasingly solution-like with rising annealing temperature despite the fact that all systems have been quenched to 300 K. Hence theory suggests that the annealing and cooling protocol can strongly influence the electronic properties of a bulk heterojunction solar cell. This has indeed been demonstrated by our UV/vis spectroscopic measurements of strongly annealed thin film samples, which

confirm the trends predicted by theory. With the combined insights provided by multiscale simulation and experiment, it may be possible to develop effective tempering routines to fine-tune the electronic structure of organic semiconductor materials.

Acknowledgements

This project was partially funded by DFG within TRR 61. DHdJ would like to acknowledge financial support from the Alexander von Humboldt Foundation. The simulations were performed at the high performance computing facilities of the University of Münster. We thank Stefan Ostendorp and Gerhard Wilde, Institute of Materials Science, University of Münster for performing the DSC measurements.

References

1 G. Yu, J. Gao, J. C. Hummelen, F. Wudl and A. J. Heeger, Polymer photovoltaic cells—enhanced efficiencies *via* a network of internal donoracceptor heterojunctions, *Science*, 1995, **270**, 1789–1791.

2 W. Cai, X. Gong and Y. Cao, Polymer solar cells: Recent development and possible routes for improvement in the performance, *Sol. Energy Mater. Sol. Cells*, 2010, **94**, 114–127.

3 Y. F. Li, Molecular design of photovoltaic materials for polymer solar cells: toward suitable electronic energy levels and broad absorption, *Acc. Chem. Res.*, 2012, **45**, 723–733.

4 B. A. Collins, E. Gann, L. Guignard, X. He, C. R. McNeill and H. Ade, Molecular miscibility of polymerfullerene blends, *J. Phys. Chem. Lett.*, 2010, **1**, 3160–3166.

5 J. You, L. Dou, K. Yoshimura, T. Kato, K. Ohya, T. Moriarty, K. Emery, C.-C. Chen, J. Gao, G. Li and Y. Yang, A polymer tandem solar cell with 10.6% power conversion efficiency, *Nat. Commun.*, 2013, **4**, 1446.

6 I. A. Howard, F. Laquai, P. E. Keivanidis, R. H. Friend and N. C. Greenham, Perylene tetracarboxydiimide as an electron acceptor in organic solar cells: a study of charge generation and recombination, *J. Phys. Chem. C*, 2009, **113**, 21225–21232.

7 C. R. McNeill and N. C. Greenham, Conjugated-polymer blends for optoelectronics, *Adv. Mater.*, 2009, **21**, 3840–3850.

8 M. Sommer, S. Huettner and M. Thelakkat, Donoracceptor block copolymers for photovoltaic applications, *J. Mater. Chem.*, 2010, **20**, 10788–10797.

9 K. Ditte, W. Jiang, T. Schemme, C. Denz and Z. Wang, Innovative sensitizer dipbi outperforms pcbm, *Adv. Mater.*, 2012, **24**, 2104–2108.

10 A. Lv, S. R. Puniredd, J. Zhang, Z. Li, H. Zhu, W. Jiang, H. Dong, Y. He, L. Jiang, Y. Li, W. Pisula, Q. Meng, W. Hu and Z. Wang, High mobility, air stable, organic single crystal transistors of an n-type diperylene bisimide, *Adv. Mater.*, 2012, **24**, 2626–2630.

11 S. Rajaram, R. Shivanna, S. K. Kandappa and K. S. Narayan, Nonplanar perylene diimides as potential alternatives to fullerenes in organic solar cells, *J. Phys. Chem. Lett.*, 2012, **3**, 2405–2408.

12 X. Zhang, Z. Lu, L. Ye, C. Zhan, J. Hou, S. Zhang, B. Jiang, Y. Zhao, J. Huang, S. Zhang, Y. Liu, Q. Shi, Y. Liu and J. Yao, A potential perylene diimide dimer-based acceptor material for highly efficient solution processed non-fullerene organic solar cells with 4.03% efficiency, *Adv. Mater.*, 2013, **25**, 57915797.

13 J. T. Bloking, T. Giovenzana, A. T. Higgs, A. J. Ponec, E. T. Hoke, K. Vandewal, S. Ko, Z. Bao, A. Sellinger and M. D. McGehee, Comparing the device physics and morphology of polymer solar cells employing fullerenes and non-fullerene acceptors, *Adv. Energy Mater.*, 2014, **4**, 1301426.

14 T. V. Pho, F. M. Toma, B. J. Tremolet de Villers, S. Wang, N. D. Treat, N. D. Eisenmenger, G. M. Su, R. C. Coffin, J. D. Douglas, J. M. J. Frechet, G. C. Bazan, F. Wudl and M. L. Chabinyc, Decacyclene triimides: paving the road to universal non-fullerene acceptors for organic photovoltaics, *Adv. Energy Mater.*, 2014, **4**, 1301007.

15 Z. Lu, B. Jiang, X. Zhang, A. Tang, L. Chen, C. Zhan and J. Yao, Perylenediimide based non-fullerene solar cells with 4.34% efficiency through engineering surface donor/acceptor compositions, *Chem. Mater.*, 2014, **26**, 2907–2914.

16 W. Jiang, L. Ye, X. Li, C. Xiao, F. Tan, W. Zhao, J. Hou and Z. Wang, Baylinked perylene bisimides as promising non-fullerene acceptors for organic solar cells, *Chem. Commun.*, 2014, **50**, 1024–1026.

17 Y. Lin, Y. Wang, J. Wang, J. Hou, Y. Li, D. Zhu and X. Zhan, A star-shaped perylene diimide electron acceptor for high-performance organic solar cells, *Adv. Mater.*, 2014, **26**, 5137–5142.

18 L. Ye, W. Jiang, W. Zhao, S. Zhang, D. Qian, Z. Wang and J. Hou, Selecting a donor polymer for realizing favorable morphology in efficient nonfullerene acceptor-based solar cells, *Small*, 2014, **10**, 46584663.

19 Y. Zang, C.-Z. Li, C.-C. Chueh, S. T. Williams, W. Jiang, Z.-H. Wang, J.-S. Yu and A. K. Y. Jen, Integrated molecular, interfacial, device engineering towards high-performance non-fullerene based organic solar cells, *Adv. Mater.*, 2014, **26**, 5708–5714.

20 R. Shivanna, S. Shoaee, S. Dimitrov, S. K. Kandappa, S. Rajaram, J. R. Durrant and K. S. Narayan, Charge generation and transport in efficient organic bulk heterojunction solar cells with a perylene acceptor, *Energy Environ. Sci.*, 2014, **7**, 435–441.

21 D. W. Gehrig, S. Roland, I. A. Howard, V. Kamm, H. Mangold, D. Neher and F. Laquai, Efficiency-limiting processes in low-bandgap polymer: perylene diimide photovoltaic blends, *J. Phys. Chem. C*, 2014, **118**, 20077–20085.

22 R. Singh, E. Aluicio-Sarduy, Z. Kan, T. Ye, R. C. I. MacKenzie and P. E. Keivanidis, Fullerene-free organic solar cells with an efficiency of 3.7% based on a low-cost geometrically planar perylene diimide monomer, *J. Mater. Chem. A*, 2014, **2**, 14348–14353.

23 L. Ye, W. Jiang, W. Zhao, S. Zhang, Y. Cui, Z. Wang and J. Hou, Polymer photovoltaic cells—enhanced efficiencies *via* a network of internal donoracceptor heterojunctions, *Science*, 1995, **270**, 1789–1791.

24 M. Böckmann, D. Marx, C. Peter, L. Delle Site, K. Kremer and N. L. Doltsinis, *Phys. Chem. Chem. Phys.*, 2011, **13**, 7604–7621.

25 M. Böckmann and N. L. Doltsinis, Can excited electronic states of macromolecules with extended pi-systems be reliably predicted? A case study on P3HT, *Frontiers in Materials*, 2015, **2**, 25.

26 J. Kirkpatrick, V. Marcon, J. Nelson, K. Kremer and D. Andrienko, Charge mobility of discotic mesophases: a multiscale quantum/classical study, *Phys. Rev. Lett.*, 2007, **98**, 227402.

27 J. Nelson, J. J. Kwiatkowski, J. Kirkpatrick and J. M. Frost, Modeling charge transport in organic photovoltaic materials, *Acc. Chem. Res.*, 2009, **42**, 1768–1778.

28 R. C. I. MacKenzie, J. M. Frost and J. Nelson, A numerical study of mobility in thin films of fullerene derivatives, *J. Chem. Phys.*, 2010, **132**, 064904.

29 V. Ruehle, J. Kirkpatrick and D. Andrienko, A multiscale description of charge transport in conjugated oligomers, *J. Chem. Phys.*, 2010, **132**, 134103.

30 V. Ruehle, A. Lukyanov, F. May, M. Schrader, T. Vehoff, J. Kirkpatrick, B. Baumeier and D. Andrienko, Microscopic simulations of charge transport in disordered organic semiconductors, *J. Chem. Theory Comput.*, 2011, **7**, 3335–3345.

31 D. Andrienko, Simulations of morphology and charge transport in supramolecular organic materials, in *Supramolecular Materials for Opto-Electronics*, ed. N. Koch, RSC Smart Materials Series, Royal Society of Chemistry, 2015.

32 M. Böckmann, T. Schemme, D. H. de Jong, C. Denz, A. Heuer and N. L. Doltsinis, Structure of P3HT crystals, thin films, and solutions by UV/Vis spectral analysis, *Phys. Chem. Chem. Phys.*, 2015, **17**, 28616–28625.

33 Gromacs, 2015, http://www.gromacs.org/.

34 D. Van der Spoel, E. Lindahl, B. Hess, G. Groenhof, A. E. Mark and H. J. C. Berendsen, GROMACS: Fast, flexible, free, *J. Comput. Chem.*, 2005, **26**(16), 1701–1718.

35 G. Bussi, D. Donadio and M. Parrinello, Canonical sampling through velocity rescaling, *J. Chem. Phys.*, 2007, **126**, 014101.

36 M. Parrinello and A. Rahman, Polymorphic transitions in single crystals: A new molecular dynamics method, *J. Appl. Phys.*, 1981, **52**, 7182–7190.

37 T. A. Wassenaar, K. Pluhackova, R. A. Böckmann, S. J. Marrink and D. P. Tieleman, Going backward: A flexible geometric approach to reverse transformation from coarse grained to atomistic models, *J. Chem. Theory Comput.*, 2014, **10**(2), 676–690.

38 Martini—Coarse Grain Force Field for Biomolecular Simulations, www.cgmartini.nl.

39 S. J. Marrink and D. P. Tieleman, Perspective on the martini model, *Chem. Soc. Rev.*, 2013, **42**, 6801–6822.

40 D. Dudenko, A. Kiersnowski, J. Shu, W. Pisula, D. Sebastiani, H. W. Spiess and M. R. Hansen, A strategy for revealing the packing in semicrystalline p-conjugated polymers: Crystal structure of bulk poly-3-hexyl-thiophene (P3HT), *Angew. Chem., Int. Ed.*, 2012, **51**, 11068–11072.

41 A. K. Malde, L. Zuo, M. Breeze, M. Stroet, D. Poger, P. C. Nair, C. Oostenbrink and A. E. Mark, An automated force field topology builder (atb) and repository: version 1.0, *J. Chem. Theory Comput.*, 2011, **7**, 4026–4037.

42 S. Canzar, M. El-Kebir, R. Pool, K. Elbassioni, A. K. Malde, A. E. Mark, D. P. Geerke, L. Stougie and G. W. Klau, Charge group partitioning in biomolecular simulation, *J. Comput. Biol.*, 2013, **20**, 188–198.

43 K. B. Koziara, M. Stroet, A. K. Malde and A. E. Mark, Testing and validation of the automated topology builder (atb) version 2.0: prediction of hydration free enthalpies, *J. Comput.-Aided Mol. Des.*, 2014, **28**, 221–233.

44 M. J. Frisch, G. W. Trucks, H. B. Schlegel, G. E. Scuseria, M. A. Robb, J. R. Cheeseman, G. Scalmani, V. Barone, B. Mennucci, G. A. Petersson, H. Nakatsuji, M. Caricato, X. Li, H. P. Hratchian, A. F. Izmaylov, J. Bloino, G. Zheng, J. L. Sonnenberg, M. Hada, M. Ehara, K. Toyota, R. Fukuda, J. Hasegawa, M. Ishida, T. Nakajima, Y. Honda, O. Kitao, H. Nakai, T. Vreven, Jr., J. A. Montgomery, J. E. Peralta, F. Ogliaro, M. Bearpark, J. J. Heyd, E. Brothers, K. N. Kudin, V. N. Staroverov, R. Kobayashi, J. Normand, K. Raghavachari, A. Rendell, J. C. Burant, S. S. Iyengar, J. Tomasi, M. Cossi, N. Rega, M. J. Millam, M. Klene, J. E. Knox, J. B. Cross, V. Bakken, C. Adamo, J. Jaramillo, R. Gomperts, R. E. Stratmann, O. Yazyev, A. J. Austin, R. Cammi, C. Pomelli, J. W. Ochterski, R. L. Martin, K. Morokuma, V. G. Zakrzewski, G. A. Voth, P. Salvador, J. J. Dannenberg, S. Dapprich, A. D. Daniels, O. Farkas, J. B. Foresman, J. V. Ortiz, J. Cioslowski and D. Fox, *Gaussian 09, Revision D.01*, Gaussian, Inc., Wallingford, CT, 2009.

45 C. Adamo and V. Barone, *J. Chem. Phys.*, 1999, **110**, 6158.

46 A. Rodrigues, M. Cidália, R. Castro, A. S. F. Farinha, M. Oliveira, J. P. C. Tomé, A. V. Machado, M. M. M. Raposo, L. Hilliou and G. Bernardo, Thermal stability of P3HT and P3HT:PCBM blends in the molten state, *Polym. Test.*, 2013, **32**, 1192–1201.

47 A. Keerthi and S. Valiyaveettil, Regioisomers of perylenediimide: Synthesis, photophysical, electrochemical properties, *J. Phys. Chem. B*, 2012, **116**, 4603–4614.